AFRL-VS-TR-2002-1590

AIR PLASMA ION REACTIONS WITH ACETYLENE, BENZENE AND NAPHTHALENE FROM 298-1400K

Anthony Midey

Northeast Consortium for Engineering Education
68 Port Royal Square
Port Royal, VA 22535

June 1999

Scientific Report

AIR FORCE RESEARCH LABORATORY
Space Vehicles Directorate
29 Randolph Road
AIR FORCE MATERIEL COMMAND
HANSCOM AIR FORCE BASE MA 01731-3010

"This technical report has been reviewed and is approved for publication"

WILLIAM M. BLUMBERG
Contract Manager

GREG McKILLOP, COL, USAF
Deputy Director
Battlespace Environment Div

This report has been reviewed by the ESC Public Affairs Office (PA) and is releasable to the National Technical Information Service (NTIS).

Qualified requestors may obtain additional copies from the Defense Technical Information Center (DTIC). All others should apply to the National Technical Information Service (NTIS).

If your address has changed, if you wish to be removed from the mailing list, or if the addressee is no longer employed by your organization, please notify AFRL/VSIM, 29 Randolph Road, Hanscom AFB MA 01731-3010. This will assist us in maintaining a current mailing list.

Do not return copies of this report unless contractual obligations or notices on a specific document require that it be returned.

REPORT DOCUMENTATION PAGE

Form Approved
OMB No. 0704-0188

1. REPORT DATE (DD-MM-YYYY)	2. REPORT TYPE	3. DATES COVERED (From - To)
22 June 1999	Interim	

4. TITLE AND SUBTITLE

Air Plasma Ion Reactions with Acetylene, Benzene and Naphthalene from 298-1400 K

5a. CONTRACT NUMBER	5b. GRANT NUMBER	5c. PROGRAM ELEMENT NUMBER	5d. PROJECT NUMBER	5e. TASK NUMBER	5f. WORK UNIT NUMBER
F19628-98-C-0029		62101F	9993	GS	PE

6. AUTHOR(S)

Anthony Midey

7. PERFORMING ORGANIZATION NAME(S) AND ADDRESS(ES)

Northeast Consortium for Engineering Education, 68 Port Royal Square, Port Royal, VA 22535

8. PERFORMING ORGANIZATION REPORT NUMBER

9. SPONSORING / MONITORING AGENCY NAME(S) AND ADDRESS(ES)

Air Force Research Laboratory/VSB
29 Randolph Road
Hanscom AFBN MA 01731-3010

10. SPONSOR/MONITOR'S ACRONYM(S)

11. SPONSOR/MONITOR'S REPORT NUMBER(S)

AFRL-VS-TR-2002-1590

12. DISTRIBUTION / AVAILABILITY STATEMENT

Approved for public release: distribution unlimited

13. SUPPLEMENTARY NOTES

14. ABSTRACT

A variable temperature-selected ion flow drift tube (VT-SIFDT) and a high temperature flowing afterglow (HTFA) have been used to study ion-molecule reactions in the 163 - 1400 K temperature range. The efrects of electronic, vibrational and rotational energy on the kinetics of a wide range of reactions important in combustion chemistry have been investigated.

15. SUBJECT TERMS

Phillips Laboratory Scholar Program, variable temperature-selected ion flow drift tube, high temperature flowing afterglow, ion-molecule reactions, combustion chemistry

16. SECURITY CLASSIFICATION OF:			17. LIMITATION OF ABSTRACT	18. NUMBER OF PAGES	19a. NAME OF RESPONSIBLE PERSON
a. REPORT	b. ABSTRACT	c. THIS PAGE			William A.M. Blumberg
Unclassified	unclssified	unclassified	unlimited	25	19b. TELEPHONE NUMBER (include area code) 781-377-3601

Final Report

Anthony J. Midey, Jr.

NCEE Prime Contract -0029 from 23 June 1998 to 22 June 1999

During the aforementioned contract period, I have employed a variable temperature-selected ion flow tube (VT-SIFT) and a high temperature flowing afterglow (HTFA) to study ion-molecule reactions from 163-1400 K. This work has been conducted under the direction of Dr. Albert A. Viggiano at the Air Force Research Laboratory in the Space Vehicles Directorate (VSBP) at Hanscom AFB, MA. Plasma chemistry occurring at very high temperatures critically impacts Air Force systems. Plasmas can develop around re-entry vehicles that interfere with communications. In addition, the chemistry of the ionosphere occurs at temperatures upwards of 2000 K. Consequently, accurate modeling of ionospheric processes requires measurements of reactions at high temperatures.[1] The HTFA has been designed[2] and used to address these issues.[1, 3, 4]

The Air Force's current interest in high temperature chemistry relates to models developed to assist in the design of airbreathing hypersonic vehicle combustors that employ ion chemistry to enhance hydrocarbon fuel combustion.[5] Unfortunately, ion chemistry may also contribute to soot formation in hydrocarbon combustion.[6, 7] Only neutral molecule chemistry, however, has been in included in recent models of soot generation.[8] Accurate models thus require high temperature data for ion-molecule reactions with many different hydrocarbons, including benzene, naphthalene and acetylene. These unsaturated compounds occur as both reactants and products in combustion chemistry. The previously mentioned HTFA apparatus has subsequently been employed to address these problems. Recent modifications to the HTFA have expanded its capabilities, allowing the first measurements of branching ratios at temperatures over 700 K. The VT-SIFT and the HTFA combined permit branching ratios and rate constants to be measured from 85 to 1800 K at pressures from 0.25 to 2 torr.

The VT-SIFT operates in the following manner.[9] Ions are generated in a high pressure source region using electron impact on a source gas. The desired reactant ion is mass selected by a quadrupole mass spectrometer and injected into the flow tube. The ions are entrained in a fast flow of helium buffer gas and thermally equilibrate to the flow tube temperature, which is controlled by a combination of heating elements and cooling lines.

After equilibration, the neutral reactant is introduced. The residual reactant ions and all product ions are sampled with an orifice and are mass selected by another quadrupole mass spectrometer then detected. The rate constants are obtained using the decline of the reactant ion signal over a previously measured reaction time as a function of excess neutral reagent concentration. Pseudo-first order kinetics hold under these conditions and the rate constants are easily calculated. The branching ratios are measured in two steps to minimize mass discrimination in the mass spectrometer and to allow accurate determination of the individual reaction channels that can differ by only one mass unit. Relative errors in the rate constants are ±15% and the absolute errors are ±25%, while the relative errors in the branching ratios are ±25%.[9]

Rate constants and branching ratios are measured in the HTFA in a similar manner,[2] with a few exceptions. The HTFA has no source selection. Consequently, branching ratios can be measured only for ions that can be generated with large flows of source gas because the ions arise from interaction with high energy helium species formed in the source region. These large flows guarantee that all unwanted reactive species are consumed before the neutral reagent gas is introduced. Corrections must also be made to the branching ratios for reactive species formed in the flow tube of the HTFA (e.g., N_4^+ when making N_2^+ ions). Further corrections may arise at high temperatures where mass coincidences with the alkali ions thermionically emitted by the flow tube material occur. The uncertainties in the HTFA data[2] are similar to those in the VT-SIFT.

In light of the interest in modeling combustion processes, the kinetics of the reactions of O_2^+ and O^+ with C_2H_2 have been studied as a function of temperature. The reaction of O_2^+ with C_2H_2 has been studied from 163 to 1400 K using the VT-SIFT and the HTFA while O^+ + C_2H_2 has been studied from 163 to 500 K in the VT-SIFT. Charge transfer is the main reaction mechanism at all temperatures with both reactants, consistent with cross section measurements of Chiu et al.[10, 11] Rapid secondary reactions of $C_2H_2^+$ with remaining C_2H_2 give several hydrocarbon cations, similar to those observed by Chiu et al.[11] and others.[12] The secondary product ions undergo tertiary and quaternary reactions where the last step is association with C_2H_2. This observation is important because successive additions of hydrocarbon molecules can form large polycyclic hydrocarbons that generate soot.[6, 7]

Rate constants for O^+ and O_2^+ reactions with C_2H_2 are plotted against temperature in Figures 1a and b, respectively. The rate constants for the O^+ reactions are slow, showing a negative temperature dependence that varies as $T^{-0.71}$. Chiu et al. note that charge transfer is

slow because one of the two available channels is spin-forbidden and the other has poor Franck-Condon factors. Chiu et al. have also shown that stable reaction intermediates and other exothermic reaction channels exist besides the charge transfer channels. However, poor orbital correlation with the T-shaped reaction intermediate may preclude these other mechanisms.[10] The rate constants for O_2^+ reactions, on the other hand, proceed essentially at the collision rate independent of temperature up to 1100 K. Above this temperature, the rate constant increases, exceeding the capture collision rate at 1400 K because the capture collision cross section begins to approach the hard sphere collision cross section. The collision rate constant can be given as the product of the collision cross section and the velocity. When the collision cross section equals the hard sphere collision cross section, the collision cross section becomes constant. Thus, the collision rate constant increases with increasing velocity, giving the upward trend.

Reactions of atomic and diatomic ions with benzene (C_6H_6) have also been investigated to augment the combustion models.[13] Reactions with air plasma ions O_2^+, O^+, NO^+, N_2^+, N_4^+ and N^+ have been studied using the VT-SIFT from 250 to 500 K. Reactions of N_2^+ and O_2^+ have been further examined in the HTFA from 500 to 1400 K. The reactions with higher energy ions Kr^+ ($^2P_{3/2,\ 1/2}$), Ar^+, F^+ and Ne^+ have also been studied so that the kinetics data can be combined to compare to previous $C_6H_6^+$ dissociation studies. Rate constants and branching ratios have been measured at all temperatures, marking the first time that ion-molecule branching ratios have been determined at temperatures over 700 K. The results are given in Tables 1-3. All of the reactions proceed at the Langevin collision rate from 250-1400 K. Figure 2 shows the relative abundances of the C_n channels versus the average total energy. The average reaction energy, $\langle E_{rxn} \rangle$, at flow tube temperature T is defined by:

$$\langle E_{rxn} \rangle = RE_{react} + \langle E_{trans} \rangle + \langle E_{rot}^{netural} \rangle + \langle E_{vib}^{neutral} \rangle + \langle E_{in}^{ion} \rangle \qquad (1)$$

In the above equation, RE_{react} is the recombination energy of the reactant ion; the average translational energy, $<E_{trans}>$, is 3/2 $k_B T$; the average rotational energy in the neutral reactant, $\langle E_{rot}^{neutral} \rangle$, is 3/2 $k_B T$ for benzene; and the average reactant ion internal energy, $\langle E_{in}^{ion} \rangle$, is $k_B T$ for the diatomic reactant ions. The average neutral reactant vibrational energy, $\langle E_{vib}^{neutral} \rangle$, is an ensemble average over a Boltzmann distribution of vibrational energy levels for all modes. The average vibrational energies in the O_2^+ and N_2^+ ions at the highest temperatures in the flow tube are negligible, e. g., 0.04 eV at 1400 K. The average available benzene internal energy (rotational and vibrational) at the temperatures used in the HTFA is noted in Tables 2

and 3. Both dissociative and non-dissociative charge transfer reactions occur. NO^+ is nearly isoenergetic with benzene so an association product is also observed, more so at lower temperatures where the complex is more stable. All other ions with recombination energies less than N^+ undergo dissociative charge transfer, giving increasing fragmentation at recombination energies up to 16 eV, but only small changes at energies above 17 eV.

The major primary product ions are $C_6H_5^+$, $C_4H_4^+$ and $C_3H_3^+$ with minor $C_6H_4^+$ and $C_5H_3^+$ channels appearing as well. The branching ratios for all of the individual product channels plotted against the average total energy are given in Figures 3a-i. The breakdown curve for $C_5H_3^+$ is the first measured for this product ion. The solid lines are breakdown curves measured with photoelectron-photoion coincidence techniques[14] and the dashed lines are similar measurements made by charge transfer mass spectrometry.[15] The combined flow tube results reproduce the earlier breakdown curves well, except for a shift in the observed threshold. The N^+ results are anomalous because they reflect reactive channels, not dissociative charge transfer. The filled symbols in Figure 3 are the VT-SIFT results where the energy is mostly the recombination energy of the reactant ion, and the hollow symbols are the HTFA results where a greater fraction of the reaction energy is in internal energy of the benzene (e.g., rotations and vibrations). The results agree except for the high temperature O_2^+ data in the HTFA above 1100 K, which may indicate limited pyrolysis of the benzene or the effects of the large spread in the internal energy distribution of benzene. The isomeric forms of $C_3H_3^+$ and $C_4H_4^+$ have also been determined using the differences in reactivity for the linear and cyclic structures with CO and C_2H_2 for $C_3H_3^+$[16, 17] and with C_6H_6 for $C_4H_4^+$.[18] Only cyclic $C_3H_3^+$ occurs but a mixture of linear and cyclic $C_4H_4^+$ is present, with a slightly larger amount of $C_4H_4^+$ at the higher reaction energies. Similar reactivity studies indicate that $C_5H_3^+$ is probably cyclic form, which is lowest in energy.[19]

The current results can be combined with previous results[20-27] to establish a schematic reaction coordinate for $C_6H_6^+$ dissociation, illustrated in Figure 4. Previous studies have shown that $C_6H_4^+$, $C_6H_5^+$, $C_4H_4^+$ and $C_3H_3^+$ arise from a common intermediate and the product channels compete with each other.[24-27] Barriers exist in the exit channels that yield $C_6H_4^+$ and cyclic $C_4H_4^+$ products while no barriers exist for the linear $C_4H_4^+$, cyclic $C_3H_3^+$ and $C_6H_5^+$ products.[25] The $C_5H_3^+$ product is a small channel so it is not pictured, but it is also a primary dissociation product that should compete with the other primary products.[28, 29] The lowest energy structure is the ethynyl cyclopropene ion[19] which has a dissociation limit

similar to the $C_3H_3^+$ and $C_4H_4^+$ channels. However, the $C_5H_3^+$ experimental threshold is higher than these products, intimating that a barrier exists to forming it.

As previously mentioned, the onset of $C_6H_6^+$ dissociation is shifted higher in energy than the thresholds in the previous breakdown curves.[14, 15] When ions dissociate slowly, they may not have time to fragment before being detected. Therefore, the required energy for dissociation to occur on a given experimental timescale appears higher than the actual threshold value, producing a kinetic shift.[22] The slow fragmentation of the $C_6H_6^{+*}$ energized ion initially formed results in a kinetic shift. However, the energized ion is also collisionally stabilized by the 0.5 to 1 torr of He buffer present, exacerbating the situation. A simple kinetic model that accounts for the competition between unimolecular dissociation, radiative relaxation and collisionai quenching can be used to calculate the unimolecular dissociation rate under typical flow tube conditions. Using this rate and the unimolecular dissociation rates as a function of internal energy determined by Kuhlewind et al.,[27] the corresponding internal energy is approximately 5.5 eV. The ionization energy of benzene is 9.25 eV, giving an onset of around 14.7 eV consistent with our observed threshold. Thus, a kinetic shift and collisional quenching completely account for the threshold deviations from earlier measurements.

Analogous ion-molecule reactions with naphthalene ($C_{10}H_8$) have also been studied from 300-1400 K.[30] Tables 4 and 5 give the results from the VT-SIFT and HTFA experiments respectively. All of the reactions proceed at the Langevin collision rate from 300-1400 K. Figure 5 shows the product branching percentages for the sum of the different C_n channels relative to the average total reaction energy. As with benzene, the filled symbols are the VT-SIFT results where the energy is mostly the recombination energy of the reactant ion, and the hollow symbols are the HTFA results where a greater fraction of the reaction energy is in internal energy of the naphthalene (e.g., rotations and vibrations). Both dissociative and non-dissociative charge transfer reactions occur. The air plasma ions with recombination energies less than N_2^+ only undergo non-dissociative charge transfer, while N_2^+ and the higher energy ions give both dissociative and non-dissociative charge transfer. The fraction of dissociative charge transfer increases as the reaction energy increases as seen in Figure 5.

Figure 6 shows VT-SIFT individual product branching percentages from 300-370 K compared to breakdown curves of $C_{10}D_8^+$ measured by Rühl et al.,[31] demonstrating good qualitative agreement. This comparison is made because similar curves for $C_{10}H_8^+$ have not

been measured. Nevertheless, the appearance energies of the deuterated ion are only 0.2 eV different from the hydrogenated version,[32] so the comparisons are valid. Individual product branching percentages are plotted versus the average reaction energy for the major product channels in Figures 7-9. Comparing the HTFA data to the VT-SIFT data allows internal energy effects to be investigated. Internal energy appears to affect the reactivity differently than electronic excitation only for $C_{10}H_8^+$, $C_6H_5^+$ and $C_6H_4^+$. Unfortunately, the high temperature HTFA data must be compared with the data for F^+, a species that is highly reactive (e.g. HF formation) but is the only simple cation available in that energy range. This fact, coupled with the broad energy distributions at high temperatures, precludes any definitive statements about internal energy effects. Despite this fact, the combined results agree well with the photoionization mass spectrometry data of Jöchims et al.[33] so their proposed mechanism is adopted. The common onset at 16 eV for the $C_{10}H_7^+$, $C_{10}H_6^+$, $C_8H_6^+$ and $C_6H_6^+$ cyclic products indicates a common naphthalene-like cation intermediate yields all four ions. At energies above 18 eV, the products may arise from an open chain $C_{10}H_8^+$ intermediate.[33] However, many of these are also energetically accessible from $C_6H_6^+$ dissociation, as seen previously.[13, 34]

The $C_{10}H_7^+$ and $C_8H_6^+$ appearance energies observed are substantially higher than the well-established thermochemical values of Ho et al.[35] The flow tube data show that the appearance energy is around 15.5 eV, 3 eV greater than the literature value.[35] The long lifetime of the $C_{10}H_8^{+*}$ initially formed results in a kinetic shift as seen with $C_6H_6^{+*}$. Using the unimolecular dissociation rates vs. internal energy determined by Ho et al. for the naphthalene cation,[35] the observed value should be about 15 eV for the nominal timescale of the flow tube experiments. This value is still 1 eV less than measured. However, collisions between the helium buffer gas and excited $C_{10}H_8^{+*}$ initially formed account for the remaining discrepancy. The simple kinetic model applied under typical flow tube conditions shows that about 10 collisions with the He buffer stabilizes the $C_{10}H_8^{+*}$. Consequently, additional energy must be added to the molecule for the unimolecular dissociation rate to become faster than collisional quenching and the experimental timescale, thus the higher thresholds.[30]

The rate constants for various ion-molecule reactions with C_2H_2, C_6H_6 and $C_{10}H_8$ have been measured over a wide temperature range. The first branching ratios at high temperatures have also been measured for C_6H_6 and $C_{10}H_8$. Being able to measure branching ratios at high temperatures allows kinetics data to be measured at relevant

combustion temperatures. The long lifetimes of the aromatic molecules studied have implications for combustion models, especially for carbon growth reactions in combustion systems. Over 3 eV of internal energy above the thermochemical threshold must be added for the unimolecular decay rate of $C_{10}H_8^+$ to be observable on our experimental timescale. Larger PAH molecules will exacerbate the situation as the ion lifetimes increase with increasing size. Consequently, higher internal energies are required for fragmentation on short timescales.[36] Any theoretical predictions that include ionic PAH constituents must therefore account for the long dissociation lifetimes, as well as the pressure effects on the branching ratios introduced by collisional stabilization.

REFERENCES

1. P. M. Hierl, I. Dotan, J. V. Seeley, J. M. Van Doren, R. A. Morris and A. A. Viggiano, J. Chem. Phys. **106**, 3540-3544 (1997).

2. P. M. Hierl, J. F. Friedman, T. M. Miller, I. Dotan, M. Mendendez-Barreto, J. Seeley, J. S. Williamson, F. Dale, P. L. Mundis, R. A. Morris, J. F. Paulson and A. A. Viggiano, Rev. Sci. Inst. **67**, 2142 (1996).

3. I. Dotan, P. M. Hierl, R. A. Morris and A. A. Viggiano, Int. J. Mass Spectrom. Ion Phys. **167/168**, 223-230 (1997).

4. I. Dotan and A. A. Viggiano, J. Chem. Phys. **110**, 4730 (1999).

5. S. Williams, S. T. Arnold, R. A. Morris, L. Q. Maurice, A. A. Viggiano, P.Bench, I. Dotan, A. J. Midey, T. Morris and E. A. Sutton, 14th Intl. Symposium on Airbreathing Engines, 1999, p.

6. P. Gerhardt and K.-H. Homann, J. Phys. Chem. **94**, 5381 (1990).

7. P. Weilmunster, A. Keller and K.-H. Homann, Combust. Flame **116**, 62 (1999).

8. L. Q. Maurice, T. Edwards and R. C. Striebich, AIAA/SAE/ASE/ASME 34th Joint Propulsion Conference (1998).

9. A. A. Viggiano, R. A. Morris, F. Dale, J. F. Paulson, K. Giles, D. Smith and T. Su, J. Chem. Phys. **93**, 1149-1157 (1990).

10. Y. Chiu, R. A. Dressler, D. J. Levandier, S. Williams and E. Murad, J. Chem. Phys. **109**, 5300 (1998).

11. Y. Chiu, R. A. Dressler, D. J. Levandier, S. Williams and E. Murad, J. Chem. Phys. **110**, 4291 (1999).

12. Y. Ikezoe, S. Matsuoka, M. Takebe and A. A. Viggiano, *Gas Phase Ion-Molecule Reaction Rate Constants Through 1986* - (Maruzen Company, Ltd., Tokyo, 1987).

13. S. T. Arnold, S. Williams, I. Dotan, A. J. Midey, R. A. Morris and A. A. Viggiano, J. Phys. Chem. A submitted for publication (1999).

14. J. H. D. Eland, R. Frey, H. Schulte and B. Brehm, Intl. J. Mass Spec. and Ion Phys. **21**, 209-211 (1976).

15. B. O. Jonsson and E. Lindholm, Arkiv Fysik **39**, 65-76 (1967).

16. D. Smith and N. G. Adams, Int. J. Mass Spec and Ion Process. **76**, 307-317 (1987).

17. K. C. Smyth, S. G. Lias and P. Ausloos, Combust. Sci. Technology **28**, 147 (1982).

18. P. Ausloos, J. Am. Chem. Soc **103**, 3931 (1981).

19. K. Lammertsma and P. v. R. Schleyer, J. Am. Chem. Soc. **105**, 1049-1051 (1983).

20. W. J. v. d. Hart, Intl. J. Mass Spec & Ion Process. **171**, 269-272 (1997).

21. W. J. v. d. Hart, Int. J. Mass Spectrom. **176**, 23-38 (1998).

22. S. G. Lias, J. E. Bartmess, J. F. Liebman, J. L. Holmes, R. D. Levin and W. G. Mallard, J. Phys. Chem. Ref. Data **17, Supplement 1**, 1-861 (1988).

23. S. G. Lias, J. E. Bartmess, J. F. Liebman, J. L. Holmes, R. D. Levin and W. G. Mallard, in *NIST Chemistry WebBook, NIST Standard Reference Database Number 69* (eds. W. G. Mallard, and P. J. Linstrom) p. (http://webbook.nist.gov) (NIST, Gaithersburg, 1998).

24. T. Baer, G. D. Willett, D. Smith and J. S. Phillips, J. Chem. Phys. **70**, 4076-4085 (1979).

25. M. F. Jarrold, W. Wagner-Redeker, A. J. Illies, N. J. Kirchner and M. T. Bowers, Intl. J. Mass Spectrom. Ion Proc. **58**, 63 (1984).

26. S. J. Klippenstein, J. D. Faulk and R. C. Dunbar, J. Chem. Phys. **98**, 243 (1993).

27. H. Kuhlewind, A. Kiermeier and H. J. Neusser, J. Chem. Phys. **85**, 4427 (1986).

28. K. R. Jennings, Z. Naturforsch **22a**, 454-459 (1967).

29. C. Ottinger, Z. Naturforsch **20a**, 1229-1231 (1965).

30. A. J. Midey, S. Williams, S. T. Arnold, I. Dotan, R. A. Morris and A. A. Viggiano, Int. J. Mass Spectrom. submitted for publication (1999).

31. E. Ruhl, S. D. Price and S. Leach, J. Phys. Chem. **93**, 6312 (1989).

32. H. W. Jochims, H. Rasekh, E. Ruhl, H. Baumgartel and S. Leach, J. Phys. Chem. **97**, 1312 (1993).

33. H. W. Jochims, H. Rasekh, E. Ruhl, H. Baumgartel and S. Leach, Chem. Phys. **168**, 159 (1992).

34. R. Chawla, A. Shukla and J. Futrell, Int. J. Mass Spectrom. Ion Proc. **165/166**, 237-247 (1997).

35. Y. P. Ho, R. C. Dunbar and C. Lifshitz, J. Am. Chem. Soc. **117**, 6504 (1995).

36. H. W. Jochims, E. Ruhl, H. Baumgartel, S. Tobita and S. Leach, Astrophys. J. **420**, 307 (1994).

TABLE 1. Temperature dependent bimolecular rate constants and product branching fractions, as measured with the VT-SIFT, for reactions of benzene with various ions. Collisional rate constants, k_c, and ion recombination energies (RE) are also indicated for each reactant ion.

Reaction	Ion RE (eV)	Rate Constant x 10^{-9} cm^3 s^{-1}, (k_c) Branching Fractions				
		250 K	300 K	350 K	400 K	500 K
$NO^+ + C_6H_6 \rightarrow$ Products	9.26		1.5 (1.6)	1.4 (1.6)	1.5 (1.6)	1.5 (1.6)
$C_6H_6^+ + NO$			0.73	0.89	0.93	0.99
$C_6H_6NO^+$			0.27	0.11	0.07	0.01
$O_2^+ + C_6H_6 \rightarrow$ Products	12.07		1.4 (1.5)			1.5 (1.5)
$C_6H_6^+ + O_2$			1.00			1.00
$N_4^+ + C_6H_6 \rightarrow$ Products	12.9		1.2 (1.3)		1.2 (1.3)	1.2 (1.3)
$C_6H_6^+ + 2N_2$			>0.99		>0.99	>0.99
$O^+ + C_6H_6 \rightarrow$ Products	13.62		1.9 (2.0)			2.0 (2.0)
$C_6H_6^+ + O$			1.00			1.00
$Kr^+ (^2P_{3/2}) + C_6H_6 \rightarrow$ Products	14.00		1.1 (1.2)		1.1 (1.2)	1.2 (1.2)
$C_6H_6^+ + Kr$			1.00		1.00	1.00
$N^+ + C_6H_6 \rightarrow$ Products	14.53		2.0 (2.1)		2.0 (2.1)	2.1 (2.1)
$C_6H_6^+ + N$			0.68		0.63	0.62
$C_6H_5^+ + (NH)$			0.07		0.10	0.11
$C_6H_4^+ + (NH_2)$			0.01		0.02	0.02
$C_5H_4^+ + (H_2 + CN)$			0.07		0.06	0.05
l-$C_4H_4^+ + (CH_2CN)$			0.02		0.03	0.03
c-$C_4H_4^+ + (CH_2CN)$			0.03		0.03	0.03
c-$C_3H_3^+ + (C_2H_2 + HCN)$			0.12		0.13	0.14
$Kr^+ (^2P_{1/2}) + C_6H_6 \rightarrow$ Products	14.66		1.1 (1.2)		1.1 (1.2)	1.2 (1.2)
$C_6H_6^+ + Kr$			0.82		0.60	0.65
$C_6H_5^+ + H + Kr$			0.18		0.40	0.35

$N_2^+ + C_6H_6 \rightarrow$ Products	15.58	1.5 (1.6)	1.6 (1.6)	1.5 (1.6)	1.7 (1.6)	1.6 (1.6)
$C_6H_6^+ + N_2$		0.13	0.12	0.11	0.10	0.08
$C_6H_5^+ + H + N_2$		0.28	0.24	0.24	0.24	0.23
$C_6H_4^+ + H_2 + N_2$		0.04	0.04	0.03	0.03	0.04
$C_5H_3^+ + CH_3 + N_2$		0.01	0.02	0.02	0.02	0.04
l-$C_4H_4^+ + C_2H_2 + N_2$		0.32	0.36	0.37	0.37	0.38
c-$C_4H_4^+ + C_2H_2 + N_2$		0.04	0.05	0.05	0.06	0.05
c-$C_3H_3^+ + C_3H_3 + N_2$		0.18	0.17	0.18	0.18	0.18
$Ar^+ + C_6H_6 \rightarrow$ Products	15.76		1.3 (1.5)		1.5 (1.5)	1.5 (1.5)
$C_6H_6^+ + Ar$			0.08		0.09	0.09
$C_6H_5^+ + H + Ar$			0.18		0.15	0.18
$C_6H_4^+ + H_2 + Ar$			0.03		0.03	0.03
$C_5H_3^+ + CH_3 + Ar$			0.03		0.03	0.06
l-$C_4H_4^+ + C_2H_2 + Ar$			0.48		0.51	0.52
c-$C_4H_4^+ + C_2H_2 + Ar$			0.07		0.05	0.03
c-$C_3H_3^+ + C_3H_3 + Ar$			0.13		0.14	0.12
$F^+ + C_6H_6 \rightarrow$ Products	17.42		1.6 (1.9)			
$C_6H_6^+ + F$			0.06			
$C_6H_5^+ + (H + F)$			0.12			
$C_6H_4^+ + (H_2 + F)$			0.01			
$C_4H_3F^+ + (C_2H_3)$			0.03			
$C_5H_3^+ + (CH_3 + F)$			0.07			
l-$C_4H_4^+ + (C_2H_2 + F)$			0.24			
c-$C_4H_4^+ + (C_2H_2 + F)$			0.18			
$C_4H_3^+ + (C_2H_3 + F)$			0.09			
$C_4H_2^+ + (C_2H_4 + F)$			0.04			
c-$C_3H_3^+ + (C_3H_3 + F)$			0.16			
$Ne^+ + C_6H_6 \rightarrow$ Products	21.56		1.6 (1.8)		1.8 (1.8)	1.8 (1.8)
$C_6H_6^+ + Ne$			0.01		0.01	0.01
$C_6H_5^+ + H + Ne$			0.02		0.01	0.03
$C_6H_4^+ + H_2 + Ne$			0.02		0.02	0.01
$C_5H_3^+ + CH_3 + Ne$			0.02		0.03	0.02
$C_4H_3^+ + (C_2H_3) + Ne$			0.59		0.61	0.58
$C_4H_2^+ + (C_2H_4) + Ne$			0.09		0.13	0.12
c-$C_3H_3^+ + (C_3H_3) + Ne$			0.11		0.11	0.11
$C_2H_3^+ + (C_4H_3) + Ne$			0.07		0.06	0.07
$C_2H_2^+ + (C_4H_4) + Ne$			0.07		0.03	0.05

TABLE 2. Temperature dependent bimolecular rate constants and product branching fractions, as measured with the HTFA from 500 – 1400 K, for the reaction of benzene with O_2^+. The collisional rate constant, k_c, and the reactant internal + translational energy are also indicated for each temperature studied.

	Rate Constant x 10^{-9} cm^3 s^{-1}, (k_c) Branching Fractions				
	500 K	800 K	1000 K	1200 K	1400 K
$O_2^+ + C_6H_6 \rightarrow$ Products	1.3 (1.5)	1.5 (1.5)	1.5 (1.5)	1.6 (1.5)	1.5 (1.5)
$C_6H_6^+ + O_2$	1.00	0.97	0.96	0.93	0.91
$C_6H_5^+ + H + O_2$				0.02	0.02
$C_4H_4^+ + C_2H_2 + O_2$		0.01	0.01	0.01	0.02
$C_4H_3^+ + C_2H_3 + O_2$		0.01	0.02	0.03	0.03
$C_4H_2^+ + C_2H_4 + O_2$		0.01	0.01	0.01	0.02
Reactant Internal Energy (eV)	0.24	0.73	1.15	1.62	2.14

TABLE 3. Temperature dependent bimolecular rate constants and product branching fractions, as measured with the HTFA from 500 – 1400 K, for the reaction of benzene with N_2^+. The collisional rate constant, k_c, and the reactant internal + translational energy are also indicated for each temperature studied.

	Rate Constant x 10^{-9} cm^3 s^{-1}, (k_c) Branching Fractions			
	500K	800 K	1100 K	1400 K
$N_2^+ + C_6H_6 \rightarrow$ Products	1.6 (1.6)	1.4 (1.6)	1.6 (1.6)	1.7 (1.6)
$C_6H_6^+ + N_2$	0.06	0.08	0.07	0.11
$C_6H_5^+ + H + N_2$	0.19	0.21	0.22	0.20
$C_6H_4^+ + H_2 + N_2$	0.06	0.04	0.04	0.03
$C_5H_3^+ + CH_3 + N_2$	0.04	0.05	0.06	0.08
$C_4H_4^+ + C_2H_2 + N_2$	0.47	0.45	0.42	0.31
$C_4H_3^+ + (C_2H_3) + N_2$		0.01	0.02	0.08
$C_4H_2^+ + (C_2H_4) + N_2$		0.01	0.02	0.05
$C_3H_3^+ + C_3H_3 + N_2$	0.18	0.15	0.15	0.14
Reactant Internal Energy (eV)	0.24	0.73	1.36	2.14

Table 4. Reaction rate constants and product branching ratios for ion-molecule reactions of $C_{10}H_8$ from 300 to 500 K measured the variable temperature-selected ion flow tube. The reactant ion recombination energies are also shown. All rate constants are listed in italics and are given in units of 10^{-9} cm^3 s^{-1}. The collision rate constant, k_c, is given in brackets next to the experimental rate constants. The enthalpies of reaction, ΔH_{rxn}, are given in kJ/mol where the assumed neutral products are given in parentheses. Enthalpies given in braces have been estimated.

Reaction (Recombination Energy)	**Products**	ΔH_{rxn}, **kJ/mol**	**Rate Constant (x 10^{-9} cm^3 s^{-1}), [k_c] Branching Ratios** 300 K	325 K	370 K	500 K
$NO^+ + C_{10}H_8 \rightarrow$	Products		*1.8 [2.0]*		*1.9 [2.0]*	
(9.26 eV)	$C_{10}H_8^+ + NO$	-108	1.00		1.00	
$O_2^+ + C_{10}H_8 \rightarrow$	Products		*1.8 [1.9]*		*1.8 [1.9]*	
(12.07 eV)	$C_{10}H_8^+ + O_2$	-379	1.00		1.00	
$O^+ + C_{10}H_8 \rightarrow$	Products		*2.4 [2.6]*		*2.3 [2.6]*	
(13.62 eV)	$C_{10}H_8^+ + O$	-529	1.00		1.00	
$N^+ + C_{10}H_8 \rightarrow$	Products		*2.7 [2.7]*	*2.9 [2.7]*	*2.4 [2.7]*	
(14.53 eV)	$C_{10}H_8^+ + N$	-617	1.00	1.00	1.00	
$N_2^+ + C_{10}H_8 \rightarrow$	Products		*2.0 [2.0]*	*2.1 [2.0]*	*2.0 [2.0]*	*2.0 [2.0]*
(15.58 eV)	$C_{10}H_8^+ + N_2$	-718	1.00	1.00	1.00	0.94
	$C_8H_6^+ + (C_2H_2) + N_2$	-292				0.04
	$C_6H_6^+ + (C_4H_2) + N_2$	-238				0.02
$Ar^+ + C_{10}H_8 \rightarrow$	Products		*1.7 [1.8]*			*1.6 [1.8]*
(15.76 eV)	$C_{10}H_8^+ + Ar$	-735	0.95			0.84
	$C_8H_6^+ + (C_2H_2) + Ar$	-310	0.03			0.08
	$C_6H_6^+ + (C_4H_2) + Ar$	-256	0.01			0.04
	$C_5H_5^+ + (C_5H_3) + Ar$	{-38}	0.01			0.04
$F^+ + C_{10}H_8 \rightarrow$	Products		*1.8 [2.4]*			
(17.42 eV)	$C_{10}H_7F^+ + H$	-778	0.04			
	$C_{10}H_8^+ + F$	-895	0.15			
	$C_{10}H_7^+ + (HF)$	-1034	0.22			

	$C_{10}H_6^+ + (H_2 + F)$	-453	0.04
	$C_9H_8^+ + (CF)$	-707	0.01
	$C_9H_7^+ + (HCF)$	-711	0.01
	$C_8H_6^+ + (C_2H_2 + F)$	-470	0.28
	$C_7H_7^+ + (C_3 + HF)$	-498	0.11
	$C_6H_6^+ + (C_4H_2 + F)$	-416	0.04
	$C_6H_5^+ + (C_2H_2 + C_2HF)$	{-506}	0.06
	$C_6H_4^+ + (C_4H_4 + F)$	-132	0.02
	$C_5H_4^+ + (C_3H_3 + C_2HF)$	-47	0.01
	$C_5H_3^+ + (C_5H_5 + F)$	-95	0.01
$Ne^+ + C_{10}H_8 \rightarrow$	Products		*2.3 [2.3]*
(21.56 eV)	$C_{10}H_7^+ + H + Ne$	-863	0.12
	$C_8H_6^+ + (C_2H_2) + Ne$	-869	0.11
	$C_8H_5^+ + (C_2H_2 + H) + Ne$	{-575}	0.06
	$C_7H_5^+ + (C_3H_3) + Ne$	{-738}	0.06
	$C_7H_4^+ + (C_3H_3 + H) + Ne$	{-474}	0.01
	$C_6H_5^+ + (C_2H_2 + C_2H) + Ne$	{-368}	0.36
	$C_6H_4^+ + (C_4H_4) + Ne$	-532	0.08
	$C_5H_5^+ + (C_5H_3) + Ne$	{-598}	0.03
	$C_5H_3^+ + (C_5H_5) + Ne$	-495	0.05
	$C_4H_4^+ + (C_4H_2 + C_2H_2) + Ne$	-317	0.03
	$C_4H_2^+ + (3C_2H_2) + Ne$	-125	0.01
	$C_3H_3^+ + (C_3H_3 + C_4H_2) + Ne$	-269	0.08

Table 5. Reaction rate constants and product branching ratios for the reaction of N_2^+ and O_2^+ with $C_{10}H_8$ from 500 to 1400 K measured the high temperature flowing afterglow. The reactant ion recombination energies are also shown. All rate constants are listed in italics and are given in units of 10^{-9} cm^3 s^{-1}.The collision rate constant, k_c, is given in brackets next to the empirical rate constants. The sum of the average internal energy in eV (rotational and vibrational energy) in the naphthalene neutral is given for the temperatures used.

Reaction (Recombination Energy)	Products	Rate Constant (x 10^{-9} cm^3 s^{-1}), [k_c] Branching Ratios				
		500 K	630 K	800 K	1200 K	1400 K
Avg. $C_{10}H_8$ Internal Energy (eV)		0.47	0.77	1.07	2.46	3.19
$O_2^+ + C_{10}H_8 \rightarrow$	Products		*1.8 [1.9]*		*1.8 [1.9]*	*1.5 [1.9]*
(12.07 eV)	$C_{10}H_8^+ + O_2$		>0.99		0.97	0.95
	$C_{10}H_7^+ + H + O_2$ $C_{10}H_6^+ + H_2 + O_2$				0.01	0.02
	$C_8H_6^+ + (C_2H_2) + O_2$				0.01	0.02
	$C_9H_n^+$, $C_7H_n^+$, $C_6H_n^+$, $C_5H_n^+$, and $C_4H_n^+$				0.01	0.01
$N_2^+ + C_{10}H_8 \rightarrow$	Products	*2.0[a] [2.0]*	*1.8 [2.0]*			*1.8 [2.0]*
(15.58 eV)	$C_{10}H_8^+ + N_2$	0.96	0.84	0.63	0.44	0.28
	$C_{10}H_7^+ + H + N_2$		0.06	0.15	0.23	0.30
	$C_{10}H_6^+ + (H_2) + N_2$			0.02	0.02	0.06
	$C_8H_6^+ + (C_2H_2) + N_2$	0.04	0.08	0.16	0.24	0.27
	$C_8H_5^+ + (C_2H_2 + H) + N_2$					0.01
	$C_6H_6^+ + (C_4H_2) + N_2$		0.01	0.03	0.06	0.06
	$C_6H_5^+ + (C_2H_2 + C_2H) + N_2$					0.01
	$C_9H_n^+$, $C_7H_n^+$, $C_6H_4^+$, $C_6H_3^+$, $C_5H_n^+$, and $C_4H_n^+$		0.01	0.01	0.01	0.01

[a]Value taken from the VT-SIFT. See Table 1.

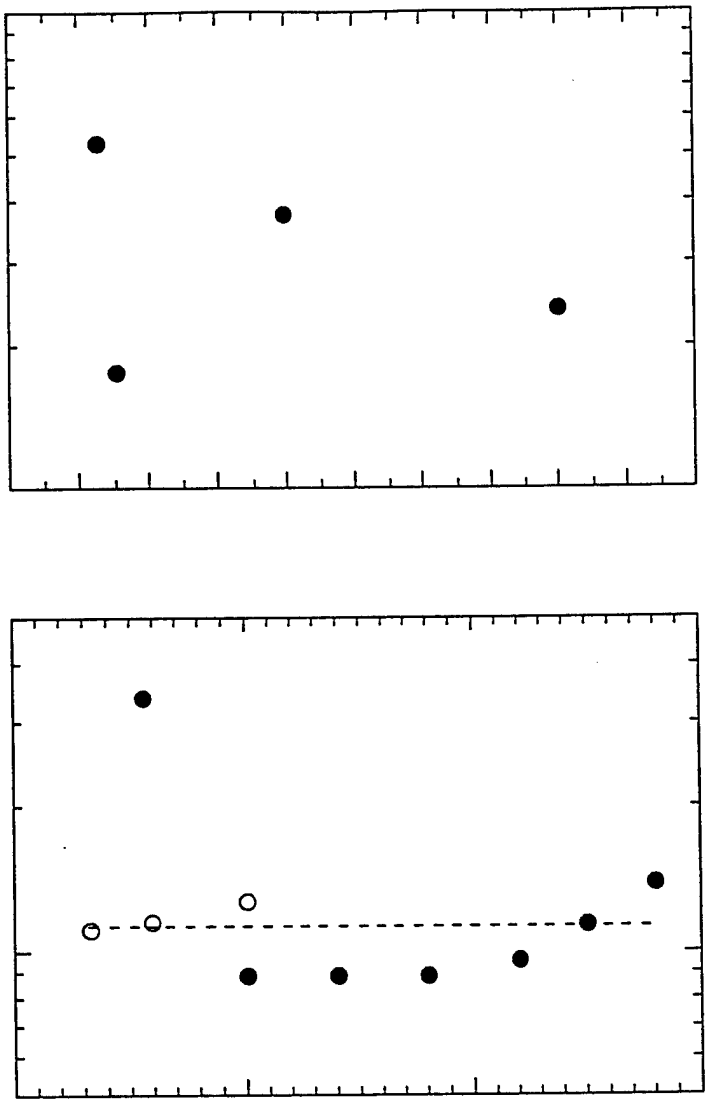

Figure 1. a) Rate constants in $cm^3\ s^{-1}$ plotted versus temperature for $O^+ + C_2H_2$ measured in the VT-SIFT.

b) Rate constants in $cm^3\ s^{-1}$ plotted versus temperature for $O_2^+ + C_2H_2$. The hollow symbols are from the VT-SIFT and the solid symbols are from the HTFA.

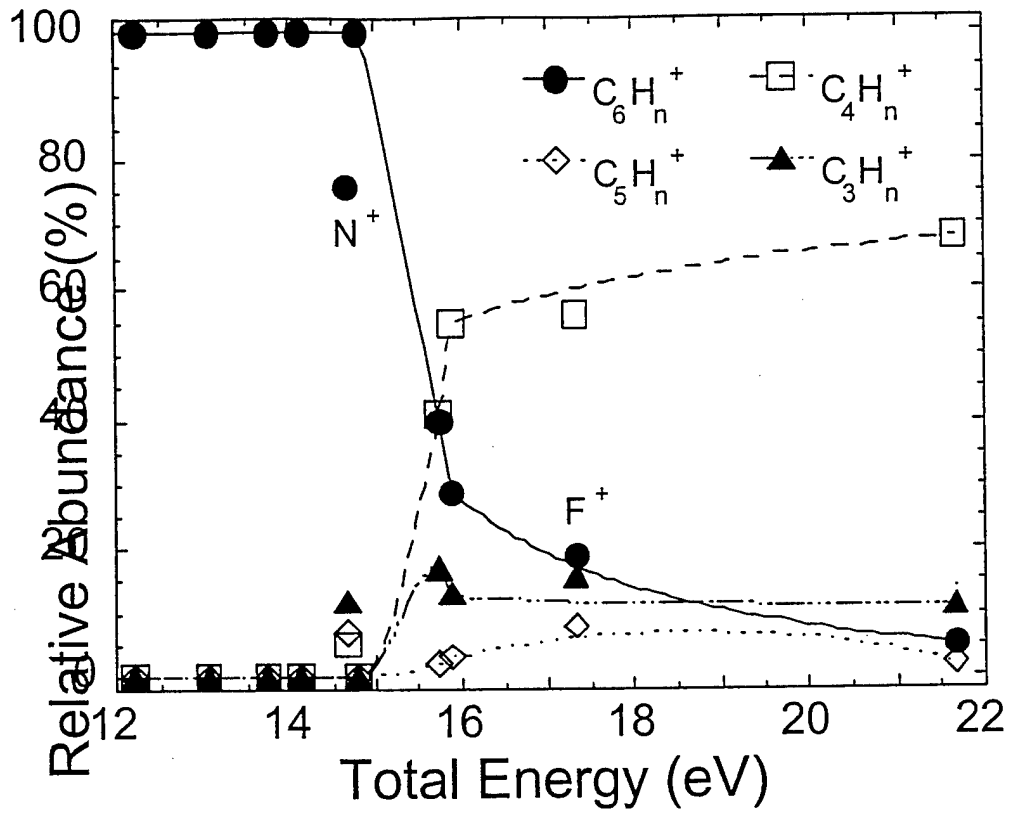

Figure 2. Simplified breakdown diagram of benzene as obtained from data in Table 1. For clarity, only 300 K data are included and products differing by one or two hydrogen atoms are grouped together. Total energy represents the sum of the ion recombination energy and the internal and translational energy of the reactants. Curves are interpolated through all data except that of the N^+ and F^+ measurements.

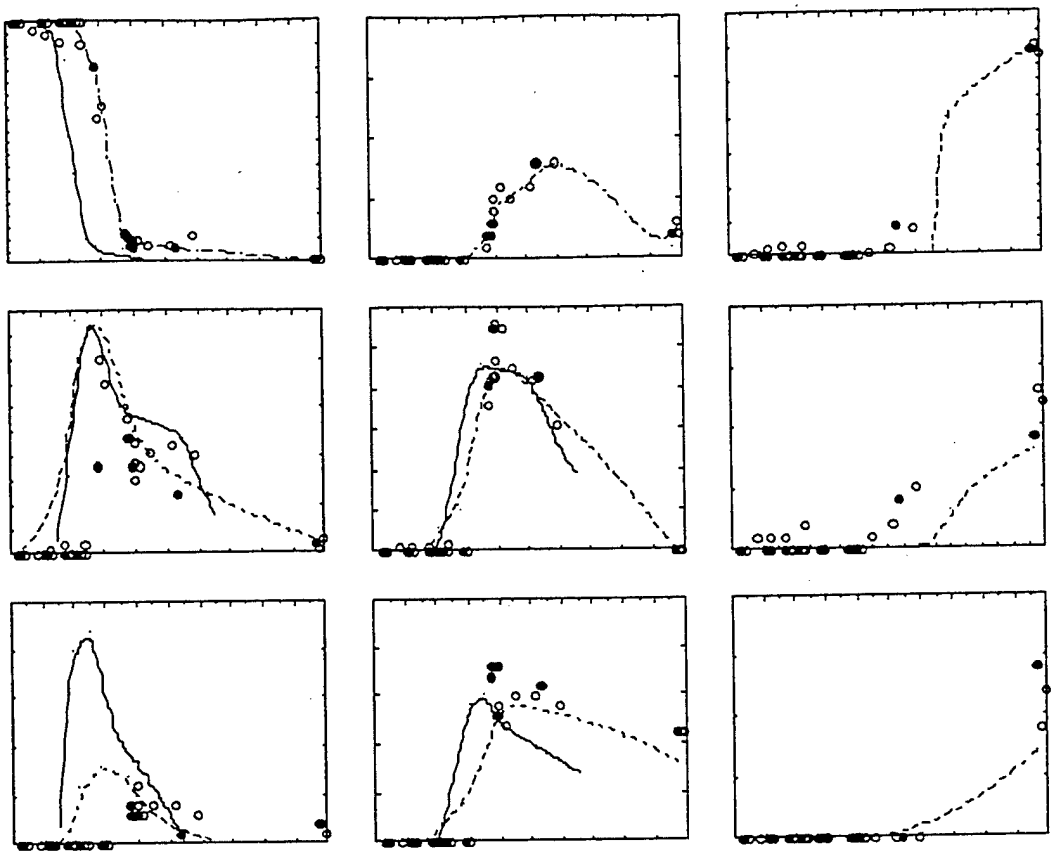

Figure 3. Breakdown curves for each product channel observed in the benzene charge transfer reactions. Solid points are 300 K SIFT data. Open points are all other temperature data from the VT-SIFT and the HTFA. The N^+ data have been excluded from the breakdown curves. Solid lines represent breakdown curves obtained previously by the photoelectron-photoion coincidence technique.[14] Dashed lines represent previous charge transfer mass spectral breakdown curves.[15] The reactant internal and translational energies have been added to the energy scale of both the photodissociation and the previous charge transfer mass spectral data. (a) $C_6H_6^+$. Dashed-dotted line is an interpolation through the 300 K SIFT data. Because the photodissociation and the previous charge transfer mass spectral data are essentially identical, only one set of previous data is shown for this channel. (b) $C_6H_5^+$. (c) $C_6H_4^+$. (d) $C_5H_3^+$. Dashed-dotted line is a smooth fit through all flow tube data. There are no previous data for comparison. (e) $C_4H_4^+$. (f) $C_3H_3^+$. (g) $C_4H_3^+$. (h) $C_4H_2^+$. (i) $C_2H_n^+$.

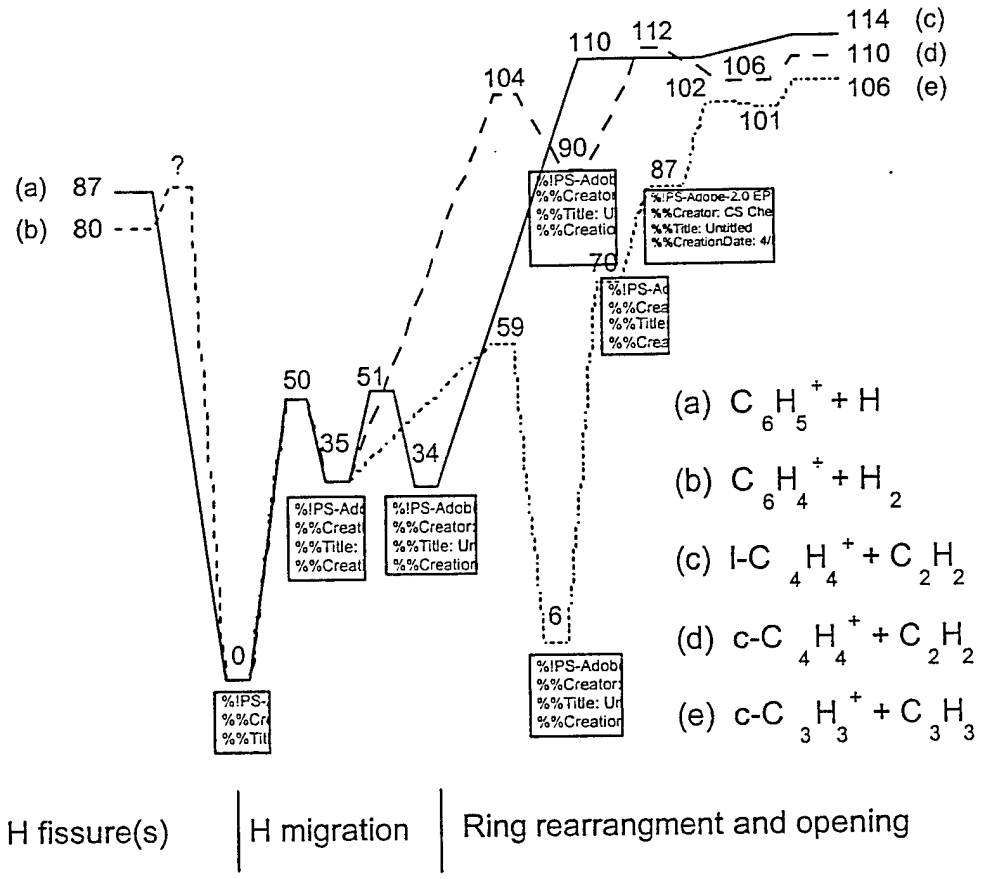

Figure 4. Schematic reaction coordinate diagram of $C_6H_6^+$ dissociation constructed from previous experimental and theoretical results as described in the text. Dissociation limits are obtained from experimental heats of formations.[22] The $C_3H_3^+$ and $C_4H_4^+$ reaction pathways are taken from van der Hart.[20, 21] Energies along the c-$C_3H_3^+$ and c-$C_4H_4^+$ pathways have been adjusted after the common intermediate to match experimental dissociation limits.

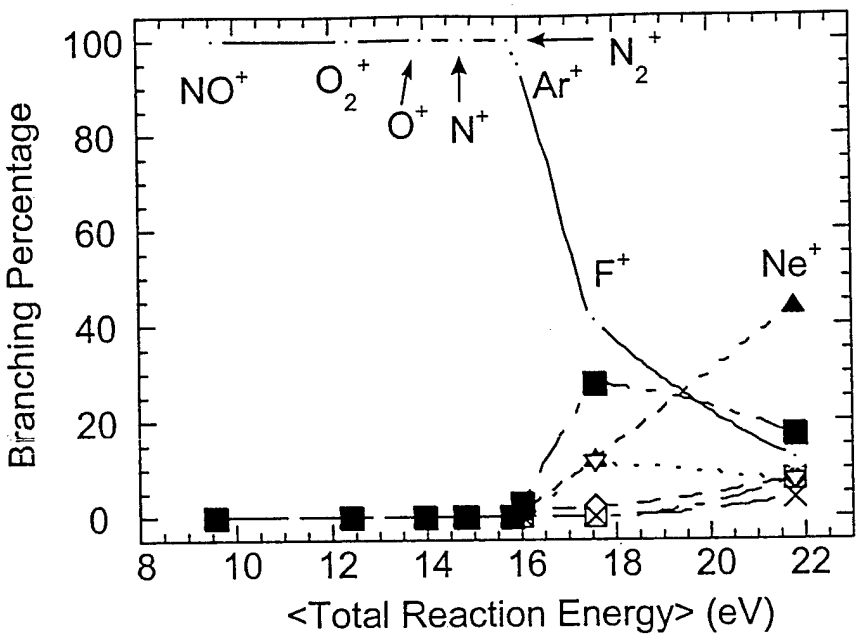

Figure 5. Branching percentages measured in the VT-SIFT for the various C_n product ion channels plotted as a function of the average total reaction energy in eV at temperatures from 300 to 370 K. The reaction energy is predominantly electronic energy in the reactant ion as determined by its recombination energy. The symbols are defined as follows: (⊙) $C_{10}H_n^+$, (■) $C_8H_n^+$, (▽) $C_7H_n^+$, (▶) $C_6H_n^+$, (◇) $C_5H_n^+$, (×) $C_4H_n^+$ and (□) $C_3H_n^+$.

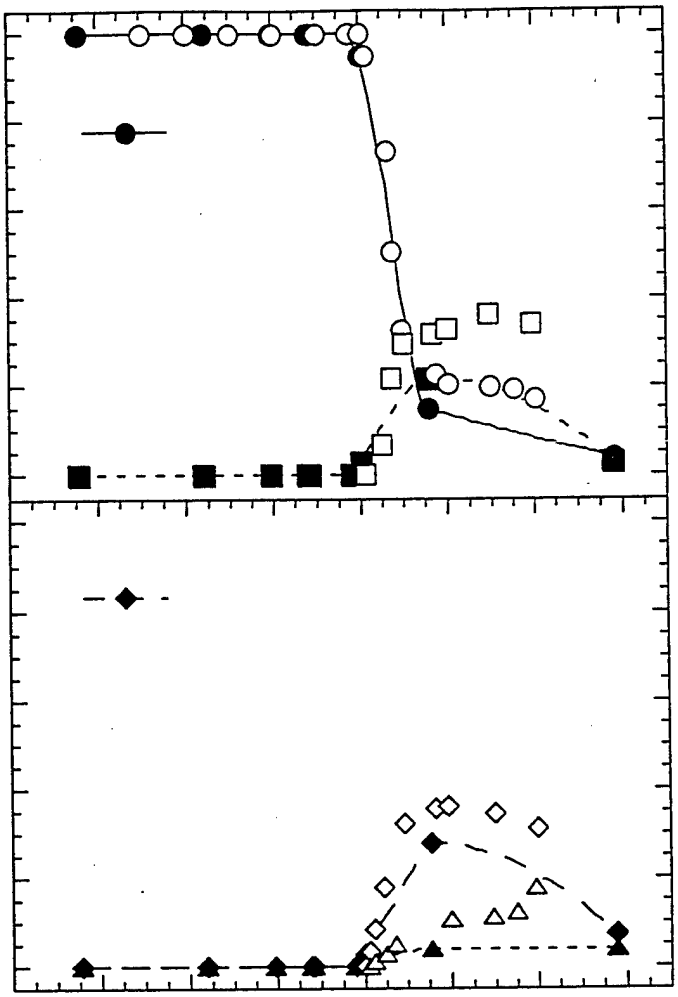

Figure 6. a) Branching percentages plotted against the average total reaction energy in eV. The symbols are defined as follows: (●) $C_{10}H_8^+$, (■) $C_{10}H_7^+$, (○) $C_{10}D_8^+$ and (□) $C_{10}D_7^+$. b) Branching percentages plotted against the average total reaction energy in eV. The symbols are defined as follows: (◆) $C_8H_6^+$, (▲) $C_6H_6^+$, (◇) $C_8D_6^+$ and (△) $C_6D_6^+$. In both plots, the solid symbols are branching percentages measured at temperatures from 300 to 370 K in the VT-SIFT, where the reaction energy is predominantly electronic energy in the reactant ion as determined by its recombination energy. The open symbols are the relative branching percentages for the deuterated product ions taken from breakdown curves measured by Rühl et al. as a function of photon energy using T-PEPICO.[31]

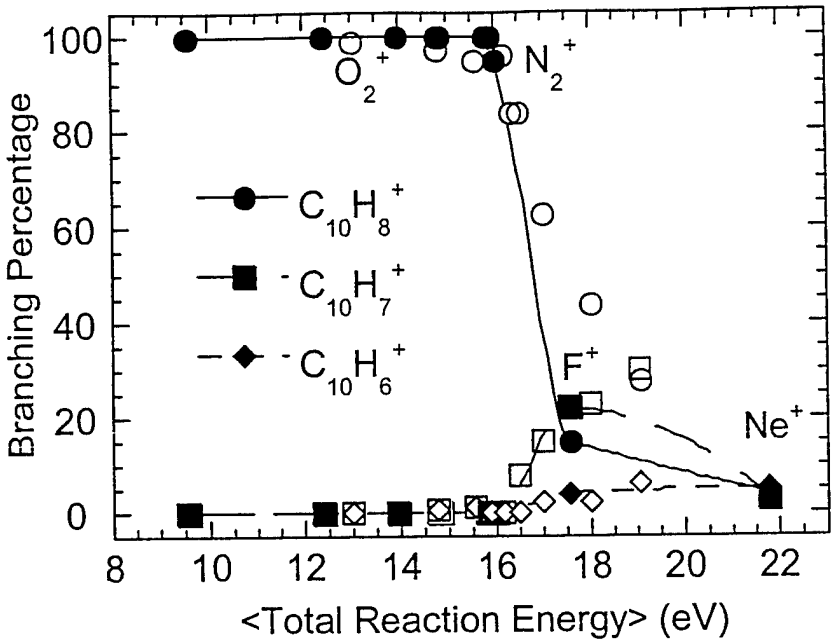

Figure 7. Branching percentages for the $C_{10}H_m^+$ product channels for m=6-8 plotted versus the average total reaction energy in eV. The solid symbols reflect primarily electronic excitation in the reactants. The open symbols reflect increasing amounts of internal excitation in vibrational and rotational energy of the reactants measured as a function of temperature from 500 to 1400 K. The symbols are defined as follows: (●) $C_{10}H_8^+$, (■) $C_{10}H_7^+$ and (◆) $C_{10}H_6^+$.

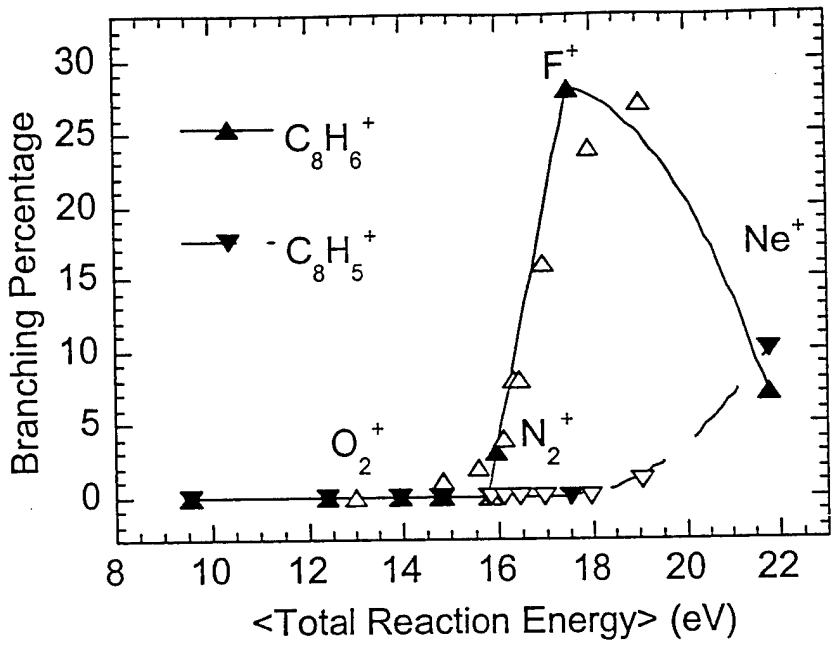

Figure 8. Branching percentages for the $C_8H_m^+$ for m=5-6 plotted versus the average total reaction energy in eV. The solid symbols reflect primarily electronic excitation in the reactants. The open symbols reflect increasing amounts of internal excitation in vibrational and rotational energy of the reactants measured as a function of temperature from 500 to 1400 K. The symbols are defined as follows: (▲) $C_8H_6^+$ and (▼) $C_8H_5^+$.

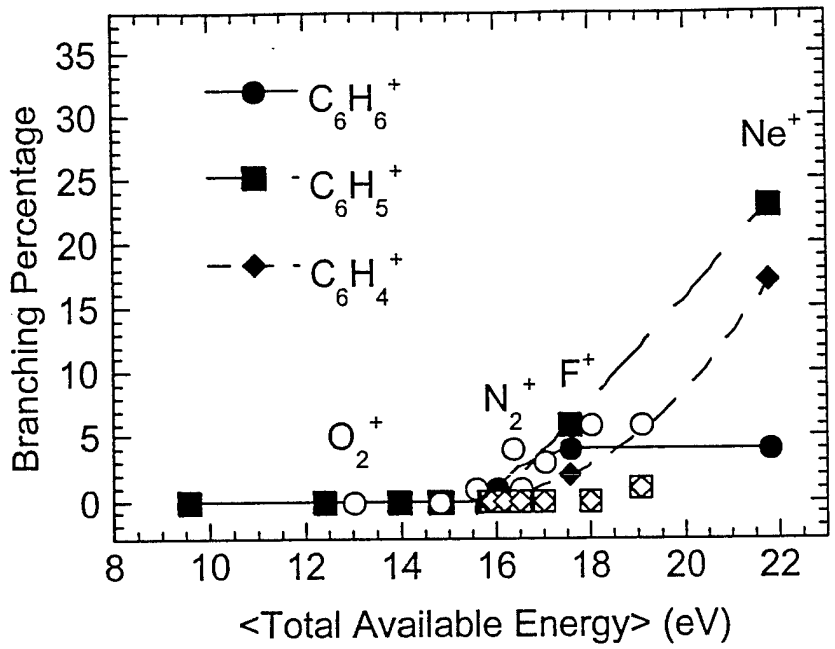

Figure 9. Branching percentages for the $C_6H_m^+$ for m=4-6 plotted versus the average total reaction energy in eV. The solid symbols reflect primarily electronic excitation in the reactants. The open symbols reflect increasing amounts of internal excitation in vibrational and rotational energy of the reactants measured as a function of temperature from 500 to 1400 K. The symbols are defined as follows: (●) $C_6H_6^+$, (■) $C_6H_5^+$ and (◆) $C_6H_4^+$